THE THERMAL STRUCTURE OF SATURN: INFERENCES FROM GROUND-BASED AND AIRBORNE INFRARED OBSERVATIONS

Alan Tokunaga

Steward Observatory, University of Arizona
Tucson, Arizona 85721

ABSTRACT

Spectroscopic and photometric infrared observations of Saturn are reviewed and compared to the expected flux from thermal structure models. Large uncertainties exist in the far-infrared measurements, but the available data indicate that the effective temperature of the disk of Saturn is 90 ±5 K. The thermal structure models proposed by Tokunaga and Cess and by Gautier *et al.* (model "N") agree best with the observations. North-South limb scans of Saturn at 10 and 20 μm show that the temperature inversion is much stronger at the South polar region than at the equator.

INTRODUCTION

The importance of infrared observations of Saturn in constraining model atmospheres and identifying trace atmospheric constituents has been recently emphasized by Caldwell (1977). Since Saturn radiates nearly all of its energy at wavelengths longer than 10 μm, the infrared spectral region is particularly important in establishing the thermal structure of Saturn. It is not surprising, therefore, that the increasing quality and wavelength coverage of infrared observations has been accompanied by a corresponding increase in the number of thermal structure models. In this paper, we review observations of Saturn in the 8-1000 μm wavelength region and relate these observations to model atmospheres. In Section II, we summarize ground-based and

airborne observations of Saturn, and we critically examine uncertainties in the effective temperature of Saturn. In Section III, thermal structure models are briefly reviewed and compared to the observations.

THE EFFECTIVE TEMPERATURE OF SATURN

One of the fundamental input parameters in an interior and atmospheric model for Saturn is the effective temperature. This is a particularly difficult quantity to measure in the case of Saturn because most of its radiant energy is in the far-infrared, a spectral region which is almost totally inaccessible to ground-based observatories. Observations of the brightness temperature of Saturn at wavelengths longer than 10 μm are shown in Tables 1 and 2. Work prior to 1972, not included here, is summarized by Newburn and Gulkis (1973). The far-infrared observations shown in Table 1 are particularly important since Saturn radiates approximately 80% of its energy at wavelengths longer than 30 μm. Unfortunately, the relatively small telescope aperture

Table 1. Airborne and Balloon Far-Infrared Photometry[a]

λ_{eff} (μm)	$\Delta\lambda$(μm)	T_B (K)	Reference
--	30 - 45	84 ± 4	Armstrong *et al.* (1972)[b]
--	45 - 80	85 ± 2	Armstrong *et al.* (1972)[b]
--	65 - 110	89 ± 5	Armstrong *et al.* (1972)[b]
--	125 - 300	79 ± 4	Armstrong *et al.* (1972)[b]
--	30 - 300	85 ± 2	Armstrong *et al.* (1972)[b]
--	45 - 300	86 ± 2	Armstrong *et al.* (1972)[b]
--	40 - 250	90 ± 5	Fazio *et al.* (1976)
39	30 - 50	91.3 ± 2.9	Loewenstein *et al.* (1977)[c]
58	45 - 80	88.1 ± 3.3	Loewenstein *et al.* (1977)[c]
80	45 - 300	87.9 ± 3.4	Loewenstein *et al.* (1977)[c]
150	100 - 400	78.7 ± 3.0	Loewenstein *et al.* (1977)[c]
410	200 - 700	95 ± 2	Loewenstein *et al.* (1977)[c]

[a]Brightness temperatures include emission from the rings. Fractional area of the rings was 0.65 during the Armstrong *et al.* observations and 0.55 during the Loewenstein *et al.* observations.

[b]The "reconciled" values given by Wright (1976) are shown here.

[c]From Tables 2 and 3 in their paper.

Table 2. Ground-Based Infrared Photometry[a]

λ_{eff} (μm)	Δλ(μm)	T_B (K)	Reference
11	6	101 ± 3	Morrison (1974)
20	11.5	92 ± 2	Morrison (1974)
20	11.5	94 ± 3[b]	Murphy (1973)
450	≥300	205 ± 15[c]	Hudson *et al.* (1974)
21	8	92 ± 1.5	Rieke (1975)
22.5	5	93 ± 1.5	Rieke (1975)
33.5	12	91 ± 2	Rieke (1975)
17.8	1	92 ± 2	Knacke *et al.* (1975)
18.4	1	90 ± 2	Knacke *et al.* (1975)
21	6	90 ± 2	Knacke *et al.* (1975)
35	14	96 ± 6	Nolt *et al.* (1977)
39	8	98 ± 2.5	Nolt *et al.* (1977)
17.8	0.6	90.3 ± 1.5	Tokunaga *et al.* (1978)
19.8	1.7	90.7 ± 1.7	Tokunaga *et al.* (1978)
22.7	2.3	88.9 ± 1.9	Tokunaga *et al.* (1978)

[a]With the exception of the measurement by Hudson *et al.*, the photometry included here have beam sizes which are smaller than the disk of Saturn.

[b]Revised value from Nolt *et al.* (1977).

[c]Includes emission from the rings.

available with aircraft and balloon telescopes has intrinsically large diffraction which prevents a measurement of the disk of Saturn independent of its rings.

The measured far-infrared brightness temperature in Table 1 includes emission from both the disk and rings of Saturn. Loewenstein *et al.* (1977) find that the effective temperature of the disk is approximately 89 K if they assume that the disk and the A and B rings have the same brightness temperature. This is approximately consistent with the broad-band brightness temperatures of Armstrong *et al.* (1972)and Fazio *et al.* (1976), and with the ground-based observations shown in Table 2.

Spectroscopic observations of the Saturn-ring system in the 20-110 μm spectral range have been made by Erickson *et al.* (1978) and by Ward (1977). These observations are shown in Figures 1 and 2. In order to remove the contribution from the rings, both assume constant A and B ring brightness temperatures with wavelength and use the

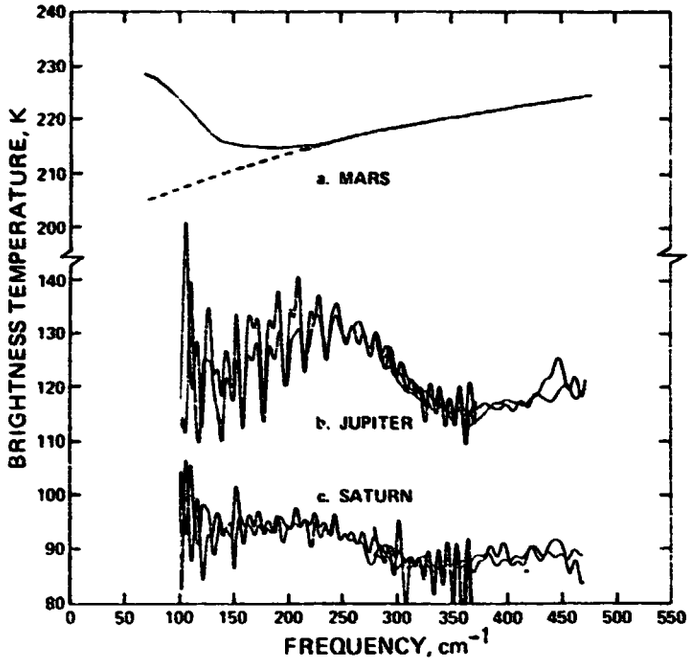

Figure 1. (a) The brightness temperature of Mars for Jan. 26, 1976 is given as a function of frequency in the solid curve. The values calculated by Wright (1976) are given by the dashed curve. (b) The average brightness temperatures for Jupiter are plotted for each of the four flights. (c) The average brightness temperatures for Saturn are plotted for each of the four flights. (From Erickson et al. 1978)

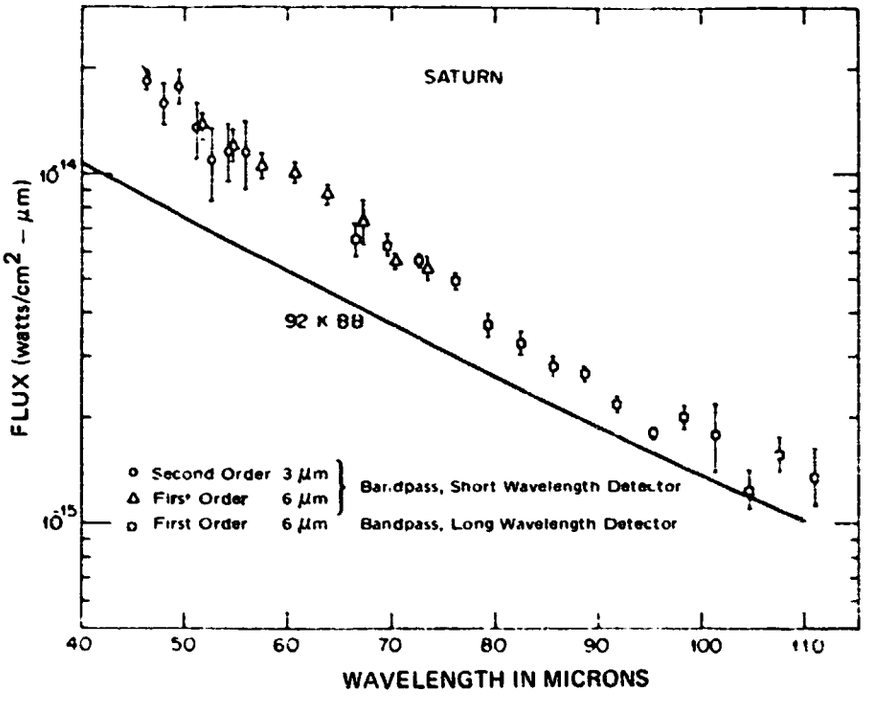

Figure 2. Flux received from Saturn and its rings. The solid line is the flux that would be received from a 92 K black body subtending the same solid angle as Saturn partially occulted by the A and B rings. (From Ward 1977)

ring optical depths given by Rieke (1975). However, Erickson *et al.* (1978) used a ring temperature of 89.3 K, while Ward used 96 K. This gives rise to a discrepancy in the effective temperature of Saturn with Erickson *et al.* (1978) finding $T_{eff} = 97 \pm 3$ K but Ward obtaining $T_{eff} = 89 \pm 3$ K. Since both groups observed Saturn in the first half of 1976, most of the disagreement in the effective temperature is probably caused by the different ring temperature used.

Ward finds the brightness temperature of Saturn, after the ring emission is removed, is 65 ± 10 K in the 80-110 μm wavelength range. Such a low brightness temperature is inconsistent with the models discussed in the next section, but Ward points out that the ring emission could be lower than he assumed if the ring particle size were small. In this case, the calculated brightness temperature of Saturn's disk could be raised. It is also possible that Mars, Ward's calibration source, may deviate from the assumed brightness temperature as predicted by Wright (1976). This possibility is raised by Erickson *et al.* who find that the brightness temperature of Mars disagrees with Wright's model at wavelengths longer than 50 μm. The increasing brightness temperature of Mars observed by Erickson *et al.*, at the longer wavelengths could partly explain the low brightness temperature of Saturn found by Ward. The validity of using Mars as a far-infrared calibration standard is clearly subject to question at the present time.

Since the ring contribution to the observed far-infrared flux is considerable, it is necessary to consider the risks involved in assuming a ring brightness equal to the disk. At the time near maximum ring tilt, Rieke (1975) found equal disk and ring brightness temperatures in the 20-34 μm spectral range, but recent observations of the rings show changes in the A, B, and C ring brightness temperature (Nolt *et al.*, 1978). We expect, therefore, that the assumption of equal ring and disk brightness temperatures to be valid only near the time of maximum ring tilt. In addition, the C ring appears to be bright in the infrared. Observations of the rings by Murphy (1973), Rieke (1975), and Nolt *et al.* (1978) find that the emission from the C ring is substantial, although Morrison (1974) did not detect it. We must therefore view with caution any correction for the ring emission at far-infrared wavelengths.

The effective temperature of Saturn is more difficult to extract from the shorter wavelength infrared data shown in Table 2. In the 8-14 μm spectral region, the continuum is greatly affected by CH_4 and C_2H_6 emission, NH_3 ice absorption, and other not yet positively identified minor constituents (Caldwell 1977, Gillett and Forrest 1974). In the 17-25 μm spectral range, the temperature inversion contributes

significantly to the observed flux (as shown in the next section). We are therefore compelled to use far-infrared data in order to obtain the effective temperature of Saturn. Any atmospheric model for Saturn, however, should be consistent with the data in Table 2.

We conclude from the available far-infrared data that the effective temperature of Saturn is 90 ± 5 K. For an equilibrium temperature of 76 K (Rieke 1975, Erickson *et al.* 1978), the ratio of emitted to absorbed power is in the range 1.6 - 2.4. Obviously more observations are necessary, and we expect that far-infrared observations in 1980, when the rings are edge-on, will provide a good value for the effective temperature. The largest experimental uncertainty will likely be in the absolute calibration.

MODEL ATMOSPHERES

We know relatively little about the thermal structure of Saturn's atmosphere compared to the Jovian atmosphere. Since Trafton (1967) first constructed a model atmosphere for Saturn, six other atmospheric models have been proposed - all within the last five years. In this section, we review the properties of these models and compare them to observations in the infrared.

The 8-14 μm spectrum of Saturn is shown in Figure 3 (Gillett and Forrest,1974). The emission peaks at 7.9 and 12.2 μm are produced by emission from methane and ethane in a temperature inversion region. Scans across the disk of Saturn in the ethane emission band (Gillett and Orton 1975) show equatorial limb brightening and an intensity enhancement at the South pole which is consistent with a temperature inversion. Saturn is not unusual in having a temperature inversion since a temperature inversion in the Jovian atmosphere has been firmly established (Gillett, Low, and Stein 1969, Gillett and Westphal 1973, Ridgway 1974) and strong evidence for a temperature inversion has been found on Titan and Neptune (Gillett 1975, Macy and Sinton 1977, and Gillett and Rieke 1977). In this paper, we assume that the absorption of solar radiation by aerosols and methane in the upper atmosphere is sufficient to power the temperature inversion (Gillett, Low, and Stein 1969, Wallace *et al.*, 1974, Caldwell 1977).

Atmospheric models by Wallace (1975), Caldwell (1977), Tokunaga and Cess (1977), and Gautier *et al.* (1977) have incorporated a temperature inversion, and these models are shown in Figure 4. The models by Cess and Khetan (1973) and by Encrenaz and Combes (1977) are similar to the Wallace (1975) model below the

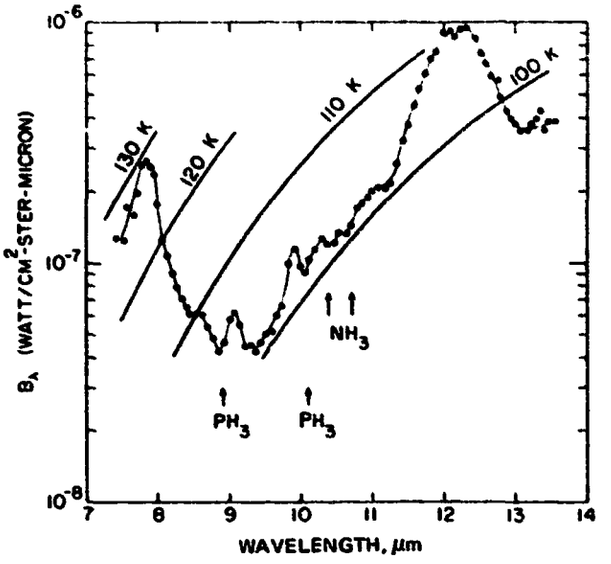

Figure 3. Surface brightness of Saturn versus wavelength. Also shown are the locations of the Q-branches of the ν_2 band of NH_3 and the ν_2 and ν_4 bands of PH_3. (From Gillett and Forrest, 1974)

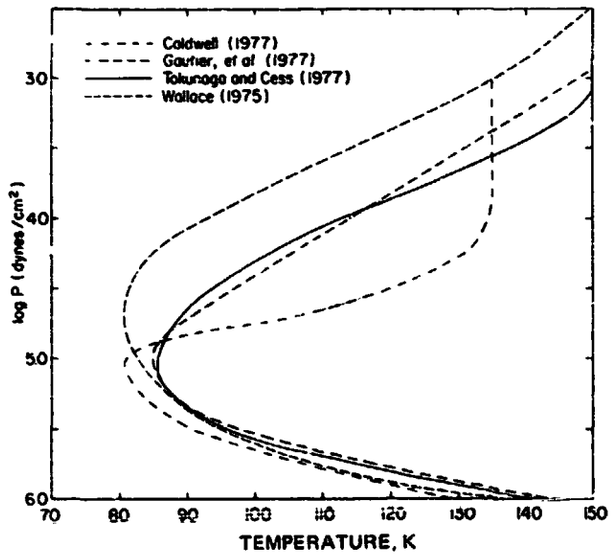

Figure 4. Thermal structure models for Saturn. The model for Tokunaga and Cess corresponds to the model in their Figure 4 (j = 0.2 and $f_E = 2 \times 10^{-6}$). The Gautier et al. *model shown is their model N.*

temperature minimum, but both models have a weaker temperature inversion (see Figure 1 of Encrenaz and Combes, 1977). The discussion of the Wallace model in this section will apply equally well to the Cess and Khetan and to the Encrenaz and Combes model. All the models, with the exception of the Wallace and the Gautier *et al.* models, have an effective temperature which is consistent with the far-infrared data discussed in the previous section. In Figure 4, it is evident that the models agree to ±10 K at any pressure level below the temperature minimum, but they are very discrepant in the temperature inversion region.

Some of the models have been compared to the far-infrared data by Erickson *et al.* (1978), as shown in Figure 5. The Tokunaga and Cess model provides a good fit throughout with a ring temperature of 89.3 K, and the Wallace model can also provide as good a fit with a higher ring temperature. The 20 μm center of disk measurements in Table 2, however, are not consistent with the Wallace model. These results depend on a uniform ring brightness temperature at all wavelengths - an assumption which may not be valid at the longer wavelengths (Ward 1977). It is important to note that the observations by Erickson *et al.* and by Ward probe to the 0.6 - 0.8 atm level in the 50-100 μm spectral range. Encrenaz and Combes (1977) show that observations of the continuum at wavelengths longer than 100 μm can test thermal structure models at higher pressures in the convective region, since the ammonia opacity is much reduced compared to Jupiter. The effect of clouds may be a serious obstacle, however.

In Figure 6, the Wallace, Caldwell, and Tokunaga and Cess models are compared to spectroscopic observations in the 17-25 μm spectral region. Observations at these wavelengths can distinguish between the various models of the temperature inversion since optical depth 1 is reached slightly below the temperature minimum. The Wallace model has a temperature inversion which is too cold, while the Caldwell model is too warm. In the latter model, the S(0) and S(1) pressure-induced rotational lines of molecular hydrogen appear slightly in emission. The Tokunaga and Cess model provides a reasonable fit to the data, and the Gautier *et al.* model "N" also fits well (see Figure 3 of their paper). The Trafton (1967) model lacks a temperature inversion, and its predicted spectrum is similar to the Wallace model. A comparison of the Tokunaga and Cess model to part of the data given in Table 2 is shown in Figure 7. This model agrees to within several standard deviations with all the disk-resolved data in the 13-40 μm spectral region.

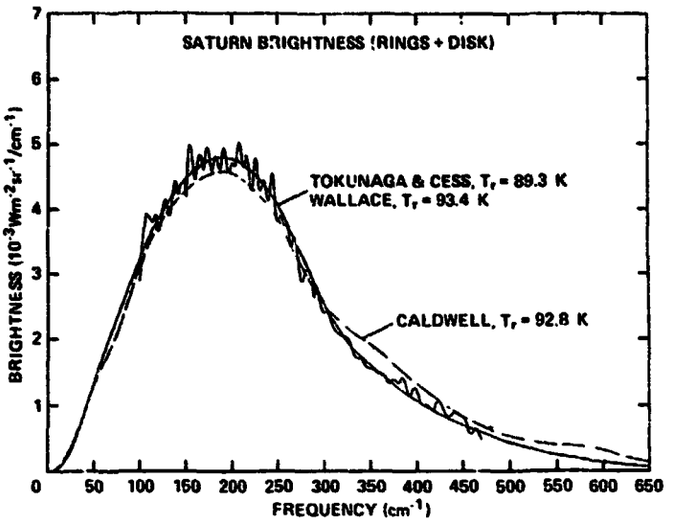

Figure 5. Comparison of observed far-infrared brightness of Saturn and its rings with model predictions. (From Erickson et al., *1978)*

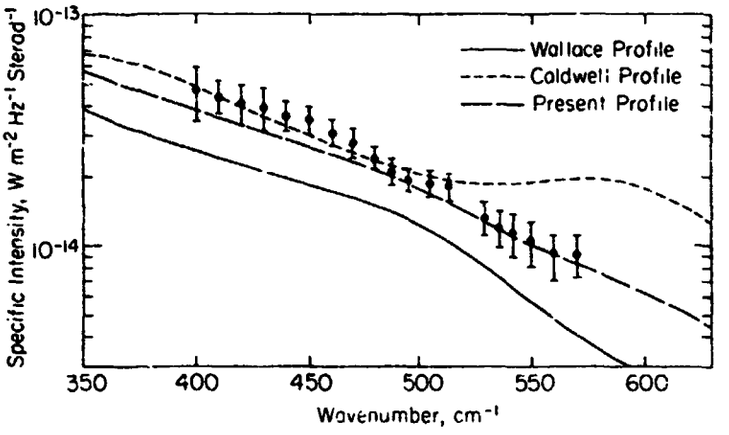

Figure 6. Comparison of the model full-disk intensities with the spectroscopic data of Tokunaga et al. *(1977). ("Present profile" refers to the Tokunaga and Cess model.) (From Tokunaga and Cess, 1977)*

The atmospheric models can also be tested by limb scans in the infrared. Caldwell *et al.* (1978) compare equatorial limb scans at three wavelengths in the 17-25 μm spectral region to the model predictions, and the results are shown in Figures 8, 9, and 10. The beam profile determined by Nolt *et al.* (1978) was used to produce the predicted limb emission profile. As a figure of merit, the deviation of the model predictions from the observed profile was computed and is shown in Table 3. Within the uncertainties in the beam profile, both the Tokunaga and Cess model and Gautier *et al* model "N" provide a good fit to the limb scans. The other models differ significantly from the observed limb profile.

We now review the evidence for differences in the thermal structure between the equatorial and the South polar region. North-South scans of the disk of Saturn at 12 and 20 μm have shown an intensity enhancement at the South polar region (Gillett and Orton, 1975; Rieke, 1975; Tokunaga *et al.*, 1978) and this effect is illustrated in Figure 11. The scans in the methane and ethane emission bands (at 7.9 and 12.2 μm) show an intensity enhancement at the South pole, but the scans in the continuum (at 11.14 and 13.31 μm) show much less limb brightening. There appears to be a slight amount of polar limb brightening at 13.31 μm, but it is not clear whether this results from molecular hydrogen or acetylene emission. The 12.2 μm scan is similar to the 12 μm scans obtained by Gillett and Orton (1975) and Rieke (1975).

The 7.9 μm scan suggests that the enhanced polar emission is mostly the result of a hotter inversion since we expect methane to be uniformly mixed over the disk of Saturn. Scans obtained in the molecular hydrogen continuum indicate that the temperature inversion is indeed hotter at the South polar region. As shown in Figure 12, the strongest limb brightening occurs at 17.8 μm, the wavelength which is closest to the maximum in the molecular hydrogen opacity. The degree of polar limb brightening can be judged by comparing Figure 12 with equatorial scans shown in Figures 8, 9, and 10.

Tokunaga *et al.* (1978) proposed a model for the South pole which was constructed in a similar fashion to the model by Tokunaga and Cess (1977), but it includes the higher acceleration of gravity at the pole and the increased value for the diurnally-averaged insolation. In Figure 13, we show the South pole model along with an equatorial model and the Tokunaga and Cess model for comparison. Note that the Tokunaga and Cess model is a global model since a diurnally-averaged insolation over all latitudes was used (for a Saturn-Sun distance of 9.5 AU). The equatorial model uses a diurnally-averaged insolation for the Saturnian equator at the time of the

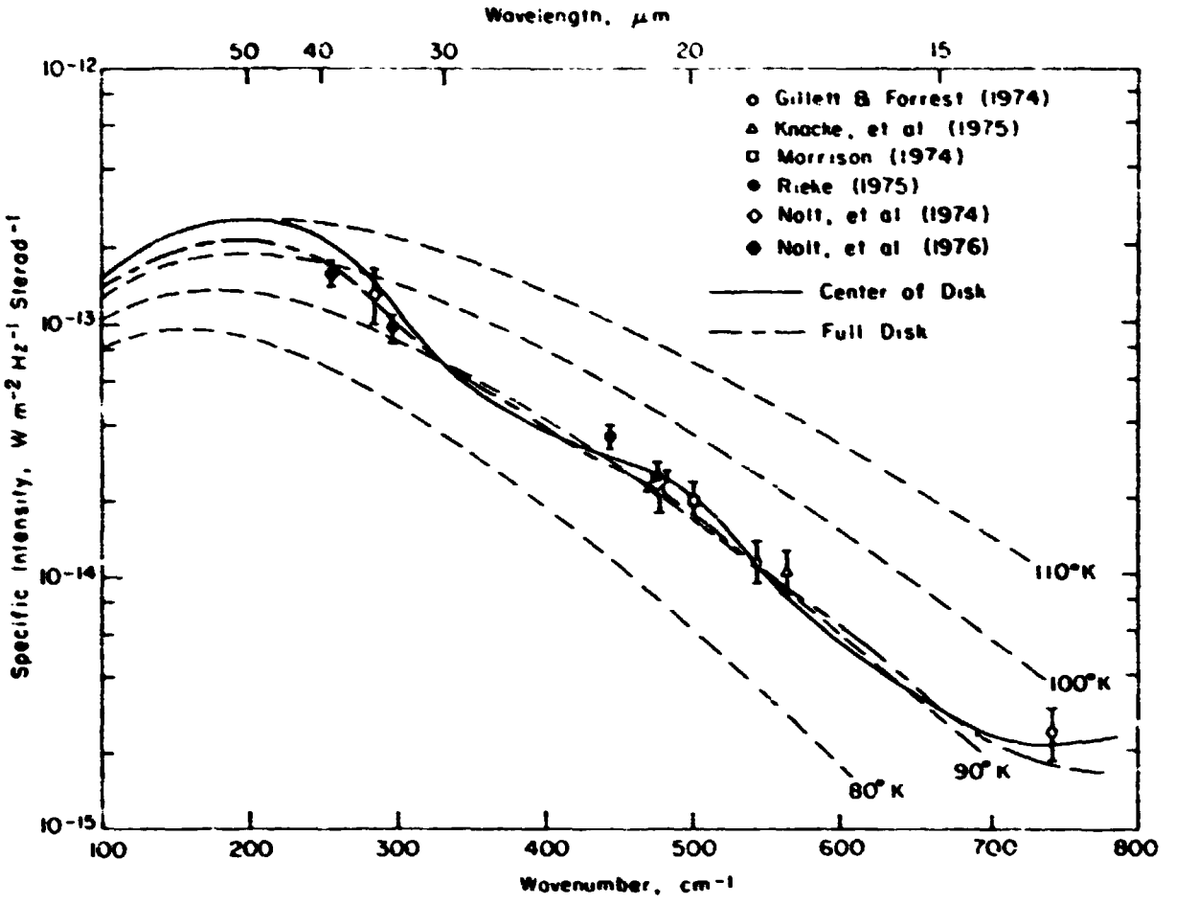

Figure 7 Comparison of the Tokunaga and Cess model with photometric data (From Tokunaga and Cess, 1977)

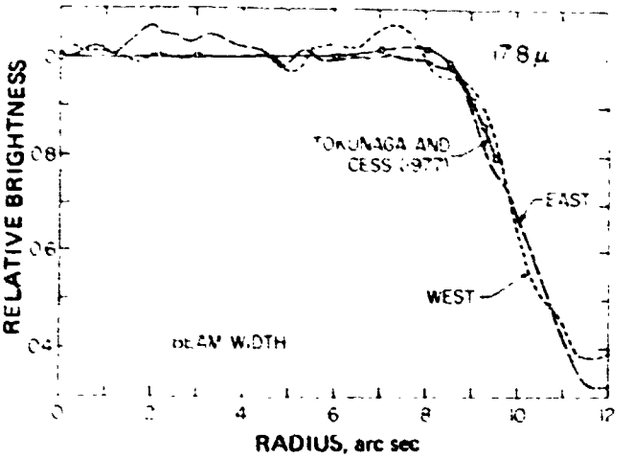

Figure 8 Center-to-limb scans near the equator of Saturn at 17.8 μm compared with the spatially smeared brightness variations from a model by Tokunaga and Cess (1977). East and West limb scans have been folded onto each other as a means of demonstrating experimental reproducibility. The signal does not go to zero at the planetary limb (10.05 arc sec) because of the ring contribution. (From Caldwell et al., 1978)

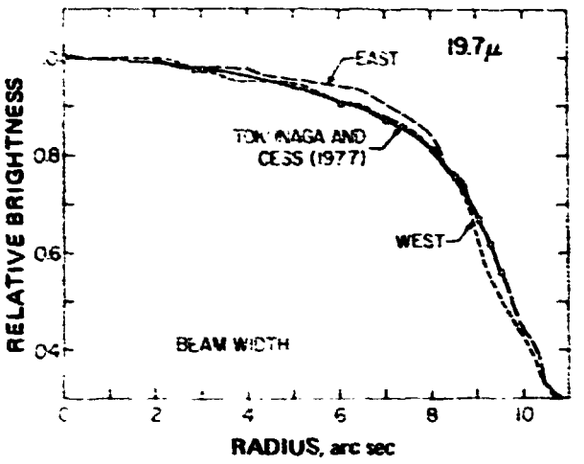

Figure 9. Center-to-limb scans near the equator of Saturn at 19.7 μm compared with the spatially smeared brightness variations from a model by Tokunaga and Cess (1977). East and West limb scans have been folded onto each other as a means of demonstrating experimental reproducibility. The signal does not go to zero at the planetary limb (10.05 arc sec) because of the ring contribution. (From Caldwell et al, 1978)

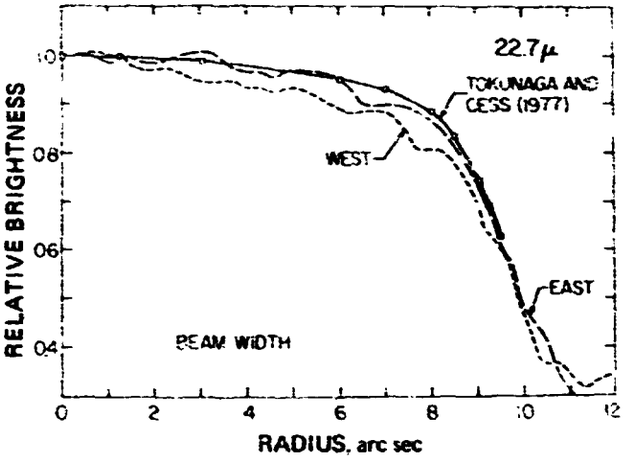

Figure 10. Center-to-limb scans near the equator of Saturn at 22.7 μm compared with the spatially smeared brightness variations from a model by Tokunaga and Cess (1977). East and West limb scans have been folded onto each other as a means of demonstrating experimental reproducibility. The signal does not go to zero at the planetary limb (10.05 arc sec) because of the ring contribution. (From Caldwell et al, 1978)

Table 3. Center to Limb Brightness Variations[1]
(from Caldwell *et al.*, 1978)

Wavelength	17.8 μm			19.7 μm			22.7 μm			RMS
Fraction of Radius from Center	0.6	0.8	0.95	0.6	0.8	0.95	0.6	0.8	0.95	
Tokunaga and Cess (1977)	-0.8	+2.2	+0.4	-2.3	-2.0	+6.1	+3.3	+3.7	+4.7	5.32
N[2]	+0.4	+5.5	+5.7	-2.4	-1.4	+8.4	+3.6	+7.4	+7.6	5.44
C	0.0	+2.8	-0.1	+3.7	+8.4	+19.8	+6.4	+10.9	+9.6	9.04
W	+4.5	+16.7	+23.0	-7.9	-7.4	+5.8	+2.9	+10.8	+16.8	12.4
N'	-1.3	-6.3	-21.3	+7.5	+8.9	+17.9	+8.7	+8.0	+3.5	11.7
C'	+6.5	+23.4	+36.9	+3.2	+12.0	+34.2	+6.6	+15.8	+23.1	23.1
W'	-1.2	-9.4	-19.2	+7.3	+12.1	+20.3	+8.7	+11.5	+5.8	12.1
Wallace (1975)	-9.8	-19.7	-33.0	-5.9	-13.1	-16.0	-1.4	-6.6	-16.6	16.1
Caldwell (1977)	+14.4	+42.6	+65.9	+9.6	+32.2	+75.8	+12.7	+33.2	+53.8	43.9

(1) [(Computed-Observed)/Observed] x 100.

(2) Models by Gautier *et al.* (1977).

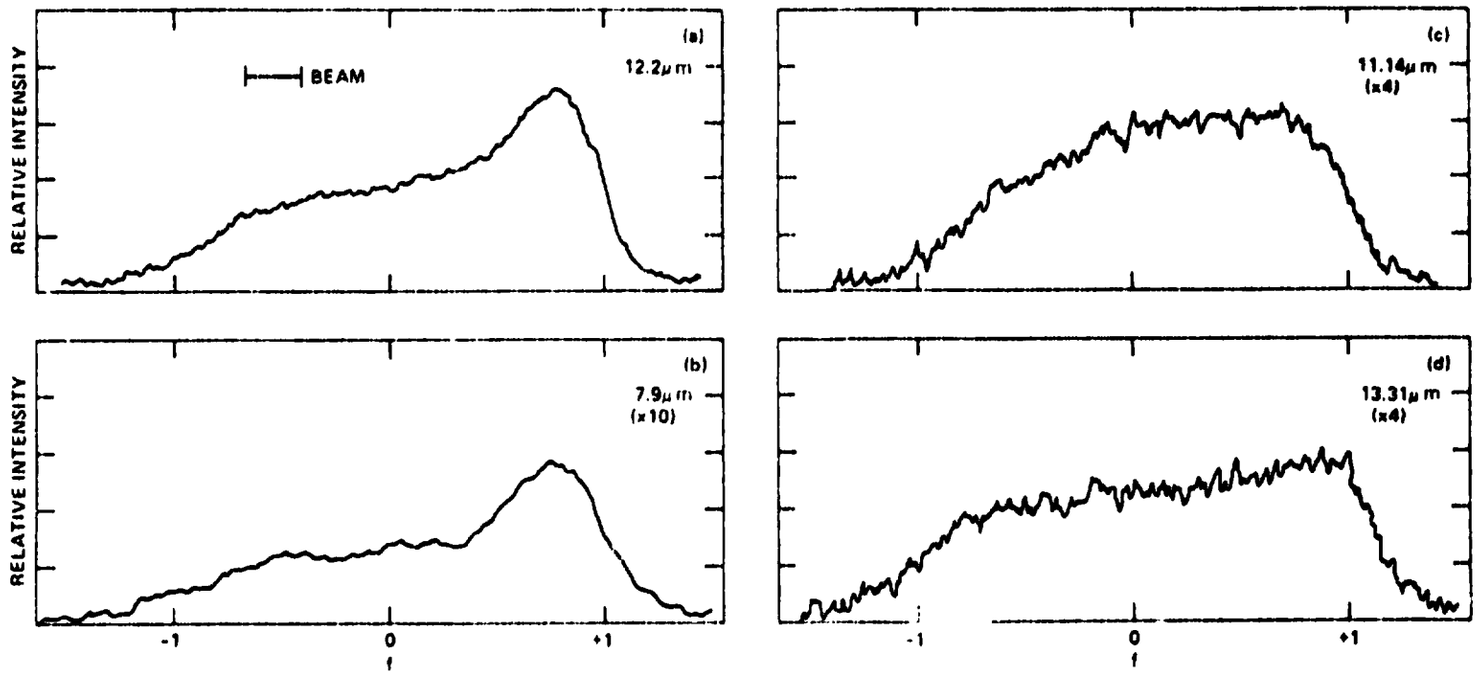

Figure 11. North-South disk scans of Saturn obtained in Feb. 1975. The abscissa is the normalized radius where 0 represents the subearth point and +1 is the southern limb of the disk. The half-power beam width for all the scans is 2.8 arc sec. The number in parenthesis is the factor by which the ordinate has been multiplied relative to Figure 11(a). The tilt to the pole toward the sun was 24.°4. (From Tokunaga et al., *1978)*

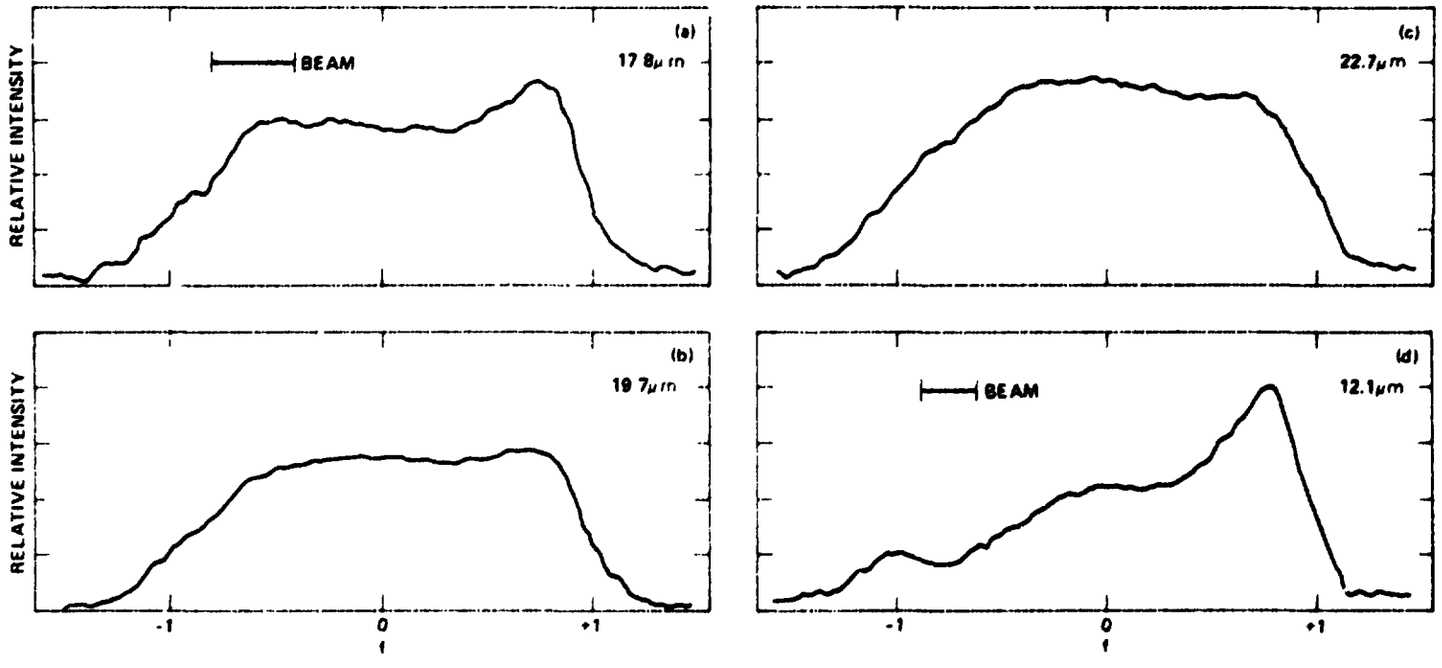

Figure 12 North-South disk scans of Saturn obtained in March 1977. The half-power beam width was 5.5 arcsec for the 20μm scans and 2.8 arc sec for the 12 μm scan. The tilt of the pole toward the sun was 16.5°. (From Tokunaga et al., 1978).

observations (9.14 AU). The South pole and equatorial models therefore have hotter temperature inversions than the global model of Tokunaga and Cess. The differences between the equatorial and global models are not large enough to affect the results obtained by Caldwell *et al.* (1978) as discussed earlier in this section.

A comparison between the predicted and observed brightness temperature for the South pole is shown in Figure 14. While the South pole model predicts a greater brightness temperature than is observed, this is partly a result of the relatively large telescope beam used (3.5 arc sec) which includes emission over a range of latitude. Tokunaga *et al.* (1978) find that at a latitude of -70° (corresponding to a distance from the pole equal to the radius of the beam), the computed temperature inversion is uniformly 3 K colder than the South pole model. From this result, roughly one-half of the brightness temperature discrepancy between the South pole model and the observations can be ascribed to beam-size effects. The South pole model appears to overestimate the heating by methane and aerosols. This result suggests that the stronger temperature inversion at the South pole could be powered with somewhat less than "normal" concentration of UV-absorbing aerosols.

We conclude that: (1) recent observational tests in the infrared favor the Tokunaga and Cess model and the Gautier *et al.* model "N", and (2) the South polar region has a stronger temperature inversion than the equatorial region. We expect that the intensity enhancement at the South pole to greatly diminish in the next few years as it tilts away from the Sun.

SUMMARY

In spite of the increasing quality of far-infrared data, the effective temperature of Saturn is not well known. Large uncertainties exist in the correction for the ring emission and in the absolute calibration. The far-infrared spectrum of Mars, the primary standard for most far-infrared observations, has only recently been measured, and more work on far-infrared calibration sources is necessary. The available far-infrared data indicates that the effective temperature of the disk of Saturn is 90 ± 5 K.

Current thermal structure models of Saturn are roughly similar in the lower atmosphere below the temperature inversion, but they differ greatly in the temperature inversion region. Ground-based observations in the 17-25 μm spectral region favor the Tokunaga and Cess (1977) model and the Gautier *et al.* (1977) model "N". There is greater uncertainty in the thermal structure below the temperature minimum, but observations at wavelengths longer than 40 μm can help to constrain models down to the

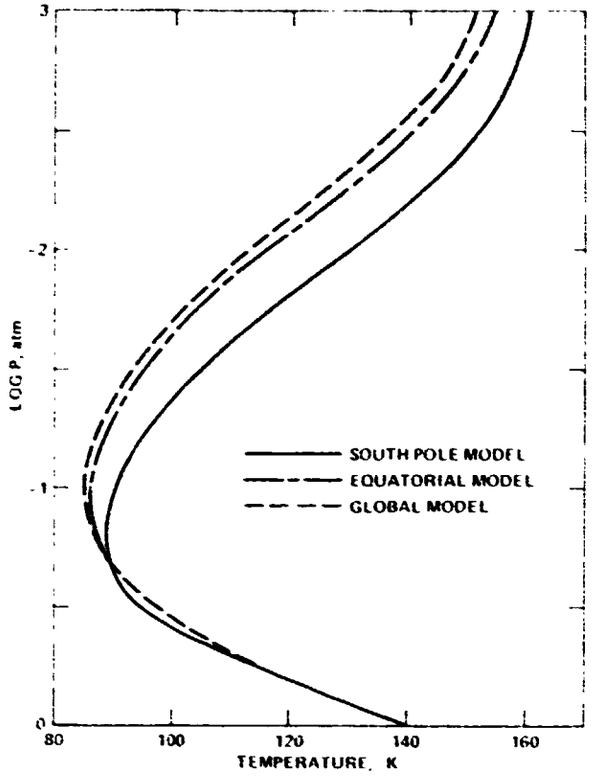

Figure 13. Models of the temperature inversion of Saturn. The global model is the same as in Tokunaga and Cess (1977) with the fraction of sunlight absorbed by aerosols = 0.2 and ethane mixing ratio = 2×10^{-6}. (From Tokunaga et al 1978)

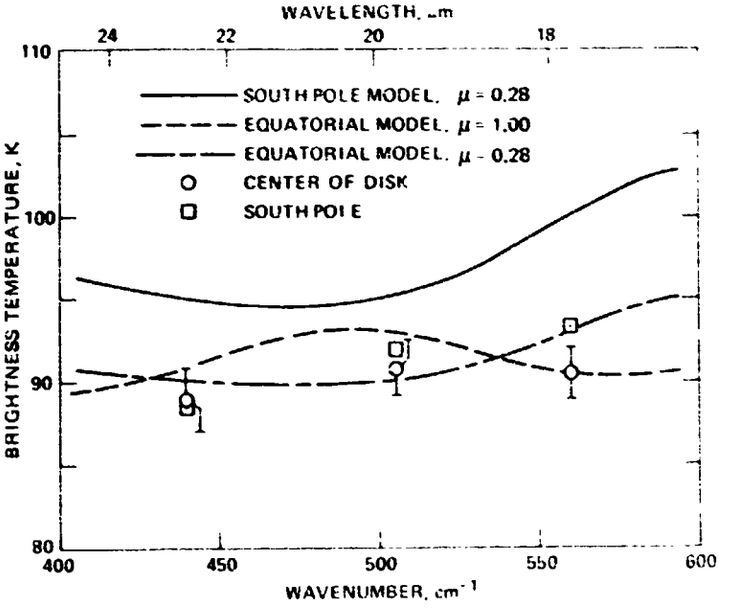

Figure 14. Comparison of the observed (see Figure 12) and model brightness temperature. The brightness temperature of the South pole model has been computed for $\mu = \cos\theta = 0.28$ where θ is the angle from the normal to the surface at which we observe Saturn. The brightness temperature of the equatorial model has been computed at the center of the disk ($\mu = 1.0$) and at the South pole ($\mu = 0.28$). (From Tokunaga et al., 1978).

cloud deck. Strong differences exist between the temperature inversion in the equatorial and the South polar regions. There are several possible ways to explain this effect, and more data concerning the deposition of solar radiation in the upper atmosphere is required.

REFERENCES

Armstrong, K. R., Harper, D. A., and Low, F. J. (1972). Far-Infrared Brightness Temperatures of the Planets. *Astrophys. J. 178*, L89–L92.

Caldwell, J. (1977). The Atmosphere of Saturn: An Infrared Perspective. *Icarus 30*, 493–510.

Caldwell, J., Gillett, F. C., Nolt, I. G., and Tokunaga, A. (1978). Spatially Resolved Infrared Observations of Saturn. I. Equatorial Limb Scans at 20 Microns. *Icarus 35*

Cess, R. D., and Khetan, S. (1973). Radiative Transfer Within the Atmospheres of the Major Planets. *J. Quant. Spectrosc. Radiat. Transfer 13*, 995–1009.

Encrenaz, T., and Combes, M. (1977). The Far-Infrared Spectrum of Saturn: Observability of PH_3 and NH_3. *Astron. Astrophys. 61*, 387–390.

Erickson, E. F., Goorvitch, D., Simpson, J. P., and Strecker, D. W. (1978). Far-Infrared Spectrophotometry of Jupiter and Saturn. *Icarus 35*, 61–73.

Fazio, F. G., Traub, W. A., Wright, E. L., Low, F. J., and Trafton, L. M. (1976). The Effective Temperature of Uranus. *Astrophys. J. 209*, 633–637.

Gautier, D., Lacombe, A., and Revah, I. (1977). Saturn: Its Thermal Profile from Infrared Measurements. *Astron. Astrophys. 61*, 149–153.

Gillett, F. C. (1975). Further Observations of the 8 - 13 Micron Spectrum of Titan. *Astrophys. J. 201*, L41–L43.

Gillett, F. C., and Forrest, W. J. (1974). The 7.5 to 13.5 Micron Spectrum of Saturn. *Astrophys. J. 187*, L37–L39.

Gillett, F. C., Low, F. J., and Stein, W. A. (1969). The 2.8 - 14 Micron Spectrum of Jupiter. *Astrophys. J. 157*, 925–934.

Gillett, F. C., and Orton, G. S. (1975). Center-to-Limb Observations of Saturn in the Thermal Infrared. *Astrophys. J. 195*, L47–L49.

Gillett, F. C., and Rieke, G. H. (1977). 5 - 20 Micron Observations of Uranus and Neptune. *Astrophys. J. 218*, L141–L144.

Gillett, F. C., and Westphal, J. A. (1973). Observations of 7.9 Micron Limb Brightening of Jupiter. *Astrophys. J. 179*, L153–L154.

Hudson, H. S., Lindsey, C. A., and Soifer, B. T. (1974). Submillimeter Observations of Planets. *Icarus 23*, 374–379.

Knacke, R. F., Owen, T., and Joyce, R. R. (1975). Infrared Observations of the Surface and Atmosphere of Titan. *Icarus 24*, 460–464.

Loewenstein, R. F., Harper, D. A., Moseley, S. H., Telesco, C. M., Thronson, H. A., Hildebrand, R. H., Whitcomb, S. E., Winston, R., and Steining, R. F. (1977). Far-Infrared and Submillimeter Observations of the Planets. *Icarus 31*, 315–324.

Macy, W., and Sinton, W. (1977). Detection of Methane and Ethane Emission on Neptune but not on Uranus. *Astrophys. J. 218*, L79–L83.

Morrison, D. (1974). Infrared Radiometry of the Rings of Saturn. *Icarus 22*, 57–65.

Murphy, R. E. (1973). Temperatures of Saturn's Rings. *Astrophys. J. 181*, L87–L90.

Newburn, R. L., and Gulkis, S. (1973). A Survey of the Outer Planets Jupiter, Saturn, Uranus, Neptune, Pluto, and their Satellites. *Space Sci. Rev. 14*, 179–271.

Nolt, I. G., Sinton, W. M., Caroff, L. J., Erickson, E. F., Strecker, D. W., and Radostitz, J. V. (1977). The Brightness Temperatures of Saturn and Its Rings at 39 Microns. *Icarus 30*, 747–759.

Nolt, I. G., Tokunaga, A., Gillett, F. C., and Caldwell, J. (1978). The 22.7 Micron Brightness of Saturn's Rings Versus Declination of the Sun. *Astrophys. J. 219*, L63–L66.

Ridgway, S. T. (1974). Jupiter: Identification of Ethane and Acetylene. *Astrophys. J. 187*, L41–L43.

Rieke, G. H. (1975). The Thermal Radiation of Saturn and Its Rings. *Icarus 26*, 37–44.

Sinton, W., and Good, J. (1977). Saturn: Predicted Seasonal Variation of Thermal Flux. *Bull. Am. Astron. Soc. 9*, 511.

Tokunaga, A., Caldwell, J., Gillett, F. C., and Nolt, I. G. (1978). Spatially Resolved Infrared Observations of Saturn. II. The Temperature Enhancement at the South Pole of Saturn. *Icarus 36*. In press.

Tokunaga, A., and Cess, R. D. (1977). A Model for the Temperature Inversion within the Atmosphere of Saturn. *Icarus 32*, 321–327.

Tokunaga, A., Knacke, R. F., and Owen, T. (1977). 17 - 25 Micron Spectra of Jupiter and Saturn. *Astrophys. J. 213*, 569–574.

Trafton, L. M. (1967). Model Atmospheres of the Major Planets. *Astrophys. J. 147*, 765–781.

Wallace, L. (1975). On the Thermal Structure of Uranus. *Icarus 25*, 538–544.

Wallace, L., Prather, M., and Belton, M. J. S. (1974). The Thermal Structure of the Atmosphere of Jupiter. *Astrophys. J. 193*, 481–493.

Ward, D. B. (1977). Far-Infrared Spectral Observations of Saturn and Its Rings. *Icarus 32*, 437–442.

Wright, E. L. (1976). Recalibration of the Far-Infrared Brightness Temperatures of the Planets. *Astrophys. J. 210*, 250–253.

DISCUSSION

G. ORTON: Do you have any estimate for the effects of this rather high and proportionately very pervasive haze (assumed to be ammonia) in the wavelengths you've been looking at?

It is a very effective absorber and scatterer in certain areas of the 8 to 14 μm region, over and above ammonia vapor absorption. One of my greatest concerns for Voyager is, what is the effect of the phenomena going to be in the far infrared which is really where we would like to get most thermal structure information, hydrogen/helium ratio, etc.

A. TOKUNAGA: We haven't addressed that question. In the 20-μm region, we don't think we see deep enough in the atmosphere of Saturn for ammonia ice opacity to affect our results.

J. CALDWELL: Optical depths in the 20-μm region at the ammonia haze level are at least 3 and typically 10 or more, at least in our model. At 17.8 μm, they're of the order of 10, so you're not seeing the effects of the haze. At very much longer wavelengths, of the order of 40 μm, it's entirely possible that on Saturn ammonia haze is a very strong contributor to the opacity. That may well foul up remote observations.

G. ORTON: I'd like to comment on the fact that we would expect to see large variations in the thermal structure, both at the equator and the pole, because of Saturn's large obliquity and the variation in insolation with time. We would like to see what sort of changes take place, what sort of equilibrium is taking place, as the insolation varies. I can say that in the 12-μm area, comparing observations made last year and this year, there is less limb brightening at the South Pole in the 12.2-μm region.

A. TOKUNAGA: We have somewhat contradictory information on that point in that we made another 12-μm scan a few weeks ago but with a smaller aperture. The brightening is about the same as you see it here. This was done a year ago. March of 1977.

J. CALDWELL: Orton is right that there are large, strong seasonal effects present. There's no indication yet of limb brightening at any wavelength in the northern hemisphere, while there's very strong limb brightening in the southern hemisphere that varies with position.

J. POLLACK: A lot of the far infrared observations that you show have been calibrated on Mars, which has become a popular standard in recent years, and particularly a lot of it has been based on very nice work by Wright (1976, *Astrophys. J. 210*, p. 250). Unfortunately, there may be a problem since Wright and others assumed that except at times of great dust storms, the atmosphere of Mars was essentially clear of dust. We now know from Viking that there is no time of the year in which that assumption can effectively be made, and that has two implications for Mars as a calibration standard in the infrared: (1) The effect of dust in the atmosphere is to reduce the ground temperature during the daytime, and that's the side that you see when you use Mars as a calibration standard. (2) The dust has significant optical depth at, say 20 μm, and will tail off at longer wavelengths, so there is a potential wavelength dependence of brightness temperature as well. I wouldn't rule Mars out as a calibration source, but I think it's going to be a lot harder to standardize.

J. CALDWELL: I think Alan Tokunaga is being a bit modest in assessing the various Saturn models. In Figure 4, the power of the limb scans is sufficient to differentiate between the two in the middle, and, in fact, Tokunaga and Cess are about twice as good as Gautier *et al.*, and in my judgment that is significant. These earlier models, including my own, were done without the limb scans. I don't think the variety you see really represents the uncertainty we now have in the models.

A. TOKUNAGA: In the 17 to 25 μm spectral region we're probing 0.2 atmosphere to about 0.05 atmosphere. We don't have very strong constraints either above or below that region. Observations in the methane band which would be sensitive to higher altitudes would be important, and with longer wavelength observations, longer than 40 μm, we can probe to lower altitudes.

G. ORTON: What is needed to determine a thermal methane/hydrogen ratio? Can we ever get observations far enough out in the wings of the 8 μm methane band, for example, to probe the same depth that can be reached in the H_2 continuum? Limb scans might be a particularly good way to relate these two opacity sources.

J. CALDWELL: If you get too far out on the wings of the methane band you also run into CH_3D opacity.